Fournet, 1955; Glatter, 1979). The inverse transform to (2.6.1.9) is given by

$$p(r) = \frac{1}{2\pi^2} \int_0^\infty I(h) hr \sin(hr)\, \mathrm{d}h \qquad (2.6.1.10)$$

or by

$$V\gamma(r) = \frac{1}{2\pi^2} \int_0^\infty I(h) h^2 \frac{\sin hr}{hr}\, \mathrm{d}h. \qquad (2.6.1.11)$$

The function $p(r)$ is directly connected with the measurable scattering intensity and is very important for the solution of the inverse scattering problem. Before working out details, we should first discuss equations (2.6.1.9) and (2.6.1.10).

The PDDF can be defined as follows: the function $p(r)$ gives the number of difference electron pairs with a mutual distance between r and $r + \mathrm{d}r$ within the particle. For homogeneous particles (constant electron density), this function has a simple and clear geometrical definition.

Let us subdivide the particle into a very large number of identical small volume elements. The function $p(r)$ is proportional to the number of lines with a length between r and $r + \mathrm{d}r$ which are found in the combination of any volume element i with any other volume element k of the particle (see Fig. 2.6.1.1). For $r = 0$, there is no other volume element, so $p(r)$ must be zero, increasing with r^2 as the number of possible neighbouring volume elements is proportional to the surface of a sphere with radius r. Starting from an arbitrary point in the particle, there is a certain probability that the surface will be reached within the distance r. This will cause the $p(r)$ function to drop below the r^2 parabola and finally the PDDF will be zero for all $r > D$, where D is the maximum dimension of the particle. So $p(r)$ is a distance histogram of the particle. There is no information about the orientation of these lines in $p(r)$, because of the spatial averaging.

In the case of inhomogeneous particles, we have to weight each line by the product of the difference in electron density $\Delta\rho$, and the differential volume element, $\mathrm{d}V$. This can lead to negative contributions to the PDDF.

We can see from equation (2.6.1.9) that every distance r gives a $\sin(hr)/(hr)$ contribution with the weight $p(r)$ to the total scattering intensity. $I(h)$ and $p(r)$ contain the same information, but in most cases it is easier to analyse in terms of distances than in terms of $\sin(x)/x$ contributions. The PDDF could be computed exactly with equation (2.6.1.10) if $I(h)$ were known for the whole reciprocal space.

For $h = 0$, we obtain from equation (2.6.1.9)

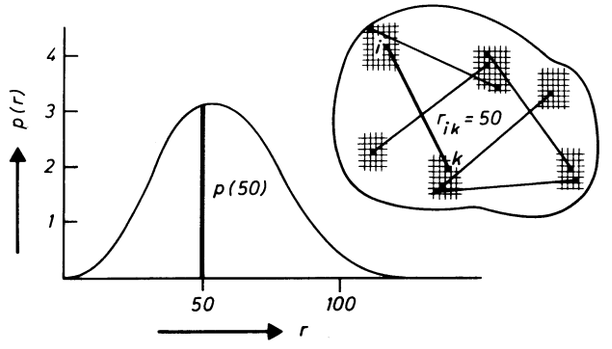

Fig. 2.6.1.1. The height of the $p(r)$ function for a certain value of r is proportional to the number of lines with a length between r and $r + \mathrm{d}r$ within the particle.

$$I(0) = I(\overline{\Delta\rho})^2 V^2 = 4\pi \int_0^\infty p(r)\, \mathrm{d}r, \qquad (2.6.1.12)$$

i.e. the scattering intensity at h equal to zero is proportional to the area under the PDDF. From equation (2.6.1.11), we find

$$V\gamma(0) = \frac{1}{2\pi^2} \int I(h) h^2\, \mathrm{d}h = V\overline{\Delta\rho^2} \qquad (2.6.1.13)$$

(Porod, 1982), *i.e.* the integral of the intensity times h^2 is related to the mean-square fluctuation of the electron density irrespective of the structure. We may modify the shape of a particle, the scattering function $I(h)$ might be altered considerably, but the integral (2.6.1.13) must remain invariant (Porod, 1951).

$$\text{Invariant } Q = \int_0^\infty I(h) h^2\, \mathrm{d}h. \qquad (2.6.1.14)$$

2.6.1.3. *Monodisperse systems*

In this subsection, we discuss scattering from monodisperse systems, *i.e.* all particles in the scattering volume have the same size, shape, and internal structure. These conditions are usually met by biological macromolecules in solution. Furthermore, we assume that these solutions are at infinite dilution, which is taken into account by measuring a series of scattering functions at different concentrations and by extrapolating these data to zero concentration. We continue with the notations defined in the previous subsection, which coincide to a large extent with the notations in the original papers and in the textbooks (Guinier & Fournet, 1955; Glatter & Kratky, 1982). There is a notation created by Luzzati (1960) that is quite different in many details. A comparison of the two notations is given in the Appendix of Pilz, Glatter & Kratky (1980).

The particles can be roughly described by some parameters that can be extracted from the scattering function. More information about the shape and structure of the particles can be found by detailed discussion of the scattering functions. At first, this discussion will be about homogeneous particles and will be followed by some aspects for inhomogeneous systems. Finally, we have to discuss the influence of finite concentrations on our results.

2.6.1.3.1. *Parameters of a particle*

Total scattering length. The scattering intensity at $h = 0$ must be equal to the square of the number of excess electrons, as follows from equations (2.6.1.7) and (2.6.1.12):

$$I(0) = (\Delta\rho)^2 V^2 = 4\pi \int_0^\infty p(r)\, \mathrm{d}r. \qquad (2.6.1.15)$$

This value is important for the determination of the molecular weight if we perform our experiments on an absolute scale (see below).

Radius of gyration. The electronic radius of gyration of the whole particle is defined in analogy to the radius of gyration in mechanics:

$$R_g^2 = \frac{\int_V \rho(r_i) r_i^2\, \mathrm{d}V_i}{\int_V \rho(r_i)\, \mathrm{d}V_i}. \qquad (2.6.1.16)$$

It can be obtained from the PDDF by

Table 2.6.1.1. *Formulae for the various parameters for h (left) and m (right) scales*

$R = K\sqrt{\tan\alpha}$ $\tan\alpha = \dfrac{\Delta \log I(h)}{\Delta h^2}$	$R = K\dfrac{\lambda a}{2\pi}\sqrt{\tan\alpha}$ $\tan\alpha = \dfrac{\Delta \log I(m)}{\Delta m^2}$
$K = \sqrt{\dfrac{3}{\log e}} = 2.628$	
$R_c = K_c\sqrt{\tan\alpha}$ $\tan\alpha = \dfrac{\Delta \log[I(h)h]}{\Delta h^2}$	$R_c = K_c\dfrac{\lambda a}{2\pi}\sqrt{\tan\alpha}$ $\tan\alpha = \dfrac{\Delta \log[I(m)m]}{\Delta m^2}$
$K_c = \sqrt{\dfrac{2}{\log e}} = 2.146$	
$R_t = K_t\sqrt{\tan\alpha}$ $\tan\alpha = \dfrac{\Delta \log[I(h)h^2]}{\Delta h^2}$	$R_t = K_t\dfrac{\lambda a}{2\pi}\sqrt{\tan\alpha}$ $\tan\alpha = \dfrac{\Delta \log[I(m)m^2]}{\Delta m^2}$
$K_t = \sqrt{\dfrac{1}{\log e}} = 1.517$	
$V = 2\pi^2\dfrac{I(0)}{Q}$ $Q = \int I(h)h^2\,\mathrm{d}h$	$V = \dfrac{\lambda^3 a^3}{4\pi}\dfrac{I(0)}{Q_m}$ $Q_m = \int I(m)m^2\,\mathrm{d}m$
$A = 2\pi\dfrac{[I(h)h]_0}{Q}$	$A = \dfrac{\lambda^2 a^2}{2\pi}\dfrac{[I(m)m]_0}{Q_m}$
$T = \pi\dfrac{[I(h)h^2]_0}{Q}$	$T = \dfrac{\lambda a}{2}\dfrac{[I(m)m^2]_0}{Q_m}$
$M = \dfrac{I(0)}{P}K\dfrac{a^2}{cd(\Delta z)^2}$	$K = \dfrac{1}{I_e N_L} = 21.0$
$M_c = \dfrac{[I(h)h]_0}{P}\dfrac{K}{\pi}\dfrac{a^2}{cd(\Delta z)^2}$	$M_c = \dfrac{[I(m)m]_0}{P}\dfrac{2K}{\lambda}\dfrac{a}{cd(\Delta z)^2}$
$M_t = \dfrac{[I(h)h^2]_0}{P}\dfrac{K}{2\pi}\dfrac{a^2}{cd(\Delta z)^2}$	$M_t = \dfrac{[I(m)m^2]_0}{P}\dfrac{2\pi K}{\lambda^2}\dfrac{1}{cd(\Delta z)^2}$
$\overline{(\Delta\rho)^2} = \dfrac{Q}{P}\dfrac{a^2}{2\pi^2 d}K$	$\overline{(\Delta\rho)^2} = \dfrac{Q_m}{P}\dfrac{4\pi}{\lambda^3 ad}K$
$K = 10^{24}/I_e$ $(10^{24} = [\mathrm{cm}/\text{Å}]^3)$	
$O_s = \pi\dfrac{K}{Q}$ $K = \lim\limits_{h\to\infty} I(h)h^4$	$O_s = \dfrac{2\pi^2}{\lambda a}\dfrac{K_m}{Q_m}$ $K = \lim\limits_{m\to\infty} I(m)m^4$

$$R_g^2 = \frac{\int_0^\infty p(r)r^2\,\mathrm{d}r}{2\int_0^\infty p(r)\,\mathrm{d}r} \qquad (2.6.1.17)$$

or from the innermost part of the scattering curve [Guinier approximation (Guinier, 1939)]:

$$I(h) = I(0)\exp(-h^2R_g^2/3). \qquad (2.6.1.18)$$

A plot of $\log[I(h)]$ *vs* h^2 (Guinier plot) shows at its innermost part a linear descent with a slope $\tan\alpha$, where

$$R_g = K\sqrt{\tan\alpha}$$

(see Table 2.6.1.1).

The radius of gyration is related to the geometrical parameters of simple homogeneous triaxial bodies as follows (Mittelbach, 1964):

sphere (radius R)	$R_g^2 = (3/5)R^2$
hollow sphere (radii R_1 and R_2)	$R_g^2 = (3/5)\dfrac{R_2^5 - R_1^5}{R_2^3 - R_1^3}$
ellipsoid (semi-axes a, b, c)	$R_g^2 = (1/5)(a^2 + b^2 + c^2)$
parallelepiped (edge lengths A, B, C)	$R_g^2 = (1/12)(A^2 + B^2 + C^2)$
elliptic cylinder (semi-axes a, b; height h)	$R_g^2 = \dfrac{a^2 + b^2}{4} + \dfrac{h^2}{12} = R_c^2 + \dfrac{h^2}{12}$
hollow cylinder (height h and radii r_1, r_2)	$R_g^2 = \dfrac{r_1^2 + r_2^2}{2} + \dfrac{h^2}{12}$.

Radius of gyration of the cross section. In the special case of rod-like particles, the two-dimensional analogue of R_g is called radius of gyration of the cross section R_c. It can be obtained from

$$R_c^2 = \frac{\int_0^\infty p_c(r)r^2\,\mathrm{d}r}{2\int_0^\infty p_c(r)\,\mathrm{d}r}, \qquad (2.6.1.19)$$

where $p_c(r)$ is the PDDF of the cross section or it can be calculated from the innermost part of the scattering intensity of the cross section $I_c(h)$:

$$I_c(h) = I_c(0)\exp(-h^2R_c^2/2), \qquad (2.6.1.20)$$

with $I_c(h) = I(h)h$ (see Table 2.6.1.1).

Radius of gyration of the thickness. A similar definition exists for lamellar particles. The one-dimensional radius of gyration of the thickness R_t can be calculated from

$$R_t^2 = \frac{\int_0^\infty p_t(r)r^2\,\mathrm{d}r}{2\int_0^\infty p_t(r)\,\mathrm{d}r}, \qquad (2.6.1.21)$$

or from the innermost part of the scattered intensity of thickness $I_t(h)$:

$$I_t(h) = I_t(0)\exp(-h^2R_t^2), \qquad (2.6.1.22)$$

with $I_t(h) = I(h)h^2$ (see Table 2.6.1.1 and §2.6.1.3.2.1).

Volume. The volume of a homogeneous particle is given by

$$V = 2\pi^2\frac{I(0)}{Q}. \qquad (2.6.1.23)$$

This equation follows from equations (2.6.1.12)–(2.6.1.14). Such volume determinations are subject to errors as they rely on the validity of an extrapolation to zero angle [to obtain $I(0)$] and to larger angles (h^{-4} extrapolation for Q). Scattering functions cannot be measured from h equal to zero to h equal to infinity.

Surface. The surface S of one particle is correlated with the scattering intensity $I_1(h)$ of this particle by

$$I_1(h)|_{h\to\infty} = (\Delta\rho)^2 \frac{2\pi}{h^4} S. \qquad (2.6.1.24)$$

Determination of the absolute intensity can be avoided if we calculate the specific surface O_s (Mittelbach & Porod, 1965)

$$O_s = S/V = \pi \frac{\lim_{h\to\infty} [I(h)h^4]}{Q}. \qquad (2.6.1.25)$$

Cross section, thickness, and correlation length. By similar equations, we can find the area A of the cross section of a rod-like particle

$$A = 2\pi \frac{[I(h)h]_{h\to 0}}{Q} \qquad (2.6.1.26)$$

and the thickness T of lamellar particles by

$$T = \pi \frac{[I(h)h^2]_{h\to 0}}{Q} \qquad (2.6.1.27)$$

but the experimental accuracy of the limiting values $[I(h)h]_{h\to 0}$ and $[I(h)h^2]_{h\to 0}$ is usually not very high.

The correlation length l_c is the mean width of the correlation function $\gamma(r)$ (Porod, 1982) and is given by

$$l_c = \frac{\pi}{Q} \int_0^\infty I(h)h \, \mathrm{d}h. \qquad (2.6.1.28)$$

The *maximum dimension* D of a particle would be another important particle parameter, but it cannot be calculated directly from the scattering function and will be discussed later.

Persistence length a_p. An important model for polymers in solution is the so-called worm-like chain (Porod, 1949; Kratky & Porod, 1949). The degree of coiling can be characterized by the persistence length a_p (Kratky, 1982*b*). Under the assumption that the persistence length is much larger than the cross section of the polymer, it is possible to find a transition point h^+ in an $I(h)h^2$ *vs* h plot where the function starts to be proportional to h. There is an approximation

$$h^+ a_p \simeq 2.3, \qquad (2.6.1.29)$$

depending on the length of the chain (Heine, Kratky & Roppert, 1962). For further details, see Kratky (1982*b*).

Molecular weight. Particles of arbitrary shape. The particle is measured at high dilution in a homogeneous solution and has an isopotential specific volume v_2' and z_2 mol. electrons per gram, *i.e.* the molecule contains $z_2 M$ electrons if M is the molecular weight. The number of effective mol. electrons per gram is given by

$$\Delta z_2 = (z_2 - v_2'\rho_0), \qquad (2.6.1.30)$$

where ρ_0 is the mean electron density of the solvent. The molecular weight can be determined from the intensity at zero angle $I(0)$:

$$M = \frac{I(0)}{P} \frac{a^2}{\Delta z^2 dc I_e N_L} = \frac{I(0)}{P} \frac{21.0a^2}{\Delta z^2 dc} \qquad (2.6.1.31)$$

(Kratky, Porod & Kahovec, 1951), where P is the total intensity per unit time irradiating the sample, a [cm] is the distance between the sample and the plane of registration, d [cm] is the thickness of the sample, c [g cm^{-3}] is the concentration, and N_L is Loschmidt's (Avogadro's) number.

Rod-like particles. The mass per unit length $M_c = M/L$, *i.e.* the mass related to the cross section of a rod-like particle with length L, is given by a similar equation (Kratky & Porod, 1953):

$$M_c = \frac{[I(h)h]_{h\to 0}}{P} \frac{a^2}{\pi \Delta z^2 dc I_e N_L} = \frac{[I(h)h]_{h\to 0}}{P} \frac{6.68a^2}{\Delta z^2 dc}. \qquad (2.6.1.32)$$

Flat particles. A similar equation holds for the mass per unit area $M_t = M/A$:

$$M_t = \frac{[I(h)h^2]_{h\to 0}}{P} \frac{a^2}{2\pi \Delta z^2 dc I_e N_L} = \frac{[I(h)h^2]_{h\to 0}}{P} \frac{3.34a^2}{\Delta z^2 dc}. \qquad (2.6.1.33)$$

Abscissa scaling. The various molecular parameters can be evaluated from scattered intensities with different abscissa scaling. The abscissa used in theoretical work is $h = (4\pi/\lambda)\sin\theta$. The most important experimental scale is m [cm], the distance of the detector from the centre of the primary beam with the distance a [cm] between the sample and the detector plane.

$$h[\mathrm{nm}^{-1}] = T_{hm}[\mathrm{cm}^{-1}\mathrm{nm}^{-1}]m[\mathrm{cm}], \qquad (2.6.1.34)$$

with

$$T_{hm} = 2\pi/\lambda a. \qquad (2.6.1.35)$$

The angular scale 2θ with

$$2\theta \simeq m/a = (\lambda/2\pi)h \qquad (2.6.1.36)$$

was used in the early years of small-angle X-ray scattering experiments. The formulae for the various parameters for m and the h scale can be found in Table 2.6.1.1, the formulae for the 2θ scale can be found in Glatter & Kratky (1982, p. 158).

2.6.1.3.2. *Shape and structure of particles*

In this subsection, we have to discuss how shape, size, and structure of the scattering particle are reflected in the scattering function $I(h)$ and in the PDDF $p(r)$. In general, it is easier to discuss features of the PDDF, but some characteristics like symmetry give more pronounced effects in reciprocal space.

2.6.1.3.2.1. *Homogeneous particles*

Globular particles. Only a few scattering problems can be solved analytically. The most trivial shape is a sphere. Here we have analytical expressions for the scattering intensity

$$I(h) = \left(3\frac{\sin(hR) - hR\cos(hR)}{(hR)^3}\right)^2 \qquad (2.6.1.37)$$

and for the PDDF (Porod, 1948)

$$p(r) = 12x^2(2 - 3x + x^3) \quad x = r/(2R) \le 1, \qquad (2.6.1.38)$$

where R is the radius of the sphere. The graphical representation of scattering functions is usually made with a semi-log plot [$\log I(h)$ *vs* h] or with a log–log plot [$\log I(h)$ *vs* $\log h$]; the PDDF is shown in a linear plot. In order to compare functions from particles of different shape, it is preferable to keep the scattering intensity at zero angle (area under PDDF) and the radius of

gyration R_g [slope of the main maximum of $I(h)$ or the second moment of $p(r)$] constant.

The scattering function of a sphere with $R = 65$ is shown in Fig. 2.6.1.2 [dashed line, $\log I(0)$ normalized to 12]. We see distinct minima which are typical for particles of high symmetry. We can determine the size of the sphere directly from the position of the zeros h_{01} and h_{02} (Glatter, 1972).

$$R \simeq \frac{4.493}{h_{01}} \quad \text{or} \quad R \simeq \frac{7.725}{h_{02}} \tag{2.6.1.39}$$

or from the position of the first side maximum ($R_g \simeq 4.5/h_1$). The minima are considerably flattened in the case of cubes (full line in Fig. 2.6.1.2). The corresponding differences in real space are not so clear-cut (Fig. 2.6.1.3). The $p(r)$ function of the sphere has a maximum near $r = R = D/2$ ($x \simeq 0.525$) and drops to zero like every PDDF at $r = D$, where D is the maximum dimension of the particle – here the diameter. The $p(r)$ for the cube with the same R_g is zero at $r \simeq 175$. The function is very flat in this region. This fact demonstrates the problems of accuracy in this determination of D when we take into account experimental errors. In any case, this accuracy will be different for different shapes.

Any deviation from spherical symmetry will shift the maximum to smaller r values and the value for D will increase [$I(0)$ and R_g constant!]. A comparison of PDDF's for a sphere, an oblate ellipsoid of revolution (axial ratio 1:1:0.2), and a prolate ellipsoid of revolution (1:1:3) is shown in Fig. 2.6.1.4. The more we change from the compact, spherical structure to a two- and one-dimensionally elongated structure, the more the maximum shifts to smaller r values and at the same time we have an increase in D. We see that $p(r)$ is a very informative function. The interpretation of scattering functions in reciprocal space is hampered by the highly abstract nature of this domain. We can see this problem in Fig. 2.6.1.5, where the scattering functions of the sphere and the ellipsoids in Fig. 2.6.1.4 are plotted. A systematic discussion of the features of $p(r)$ can be found elsewhere (Glatter, 1979, 1982*b*).

Rod-like particles. The first example of a particle elongated in one direction (prolate ellipsoid) was given in Figs. 2.6.1.4 and 2.6.1.5. An important class is particles elongated in one

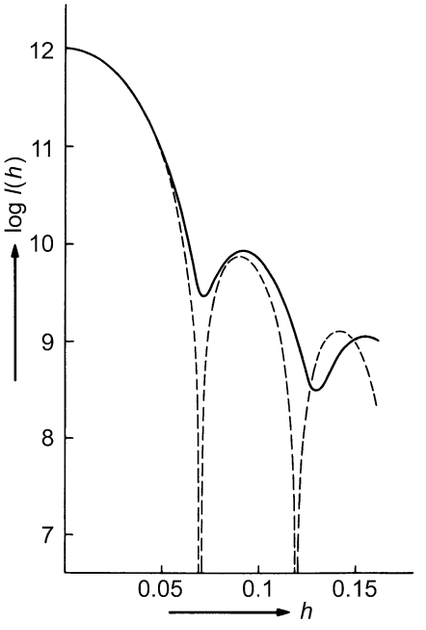

Fig. 2.6.1.2. Comparison of the scattering functions of a sphere (- - - -) and a cube (———) with same radius of gyration.

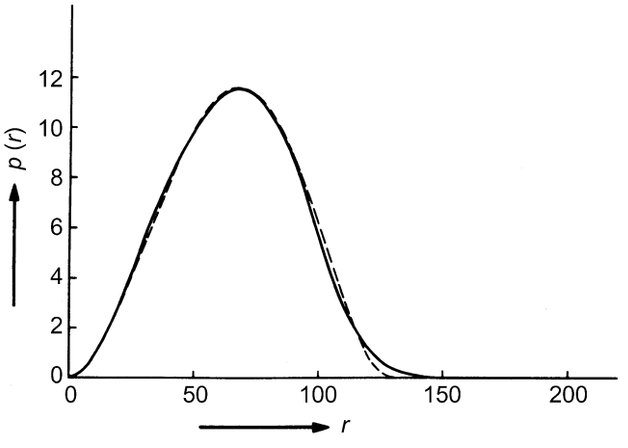

Fig. 2.6.1.3. Distance distribution function of a sphere (- - - -) and a cube (———) with the same radius of gyration and the same scattering intensity at zero angle.

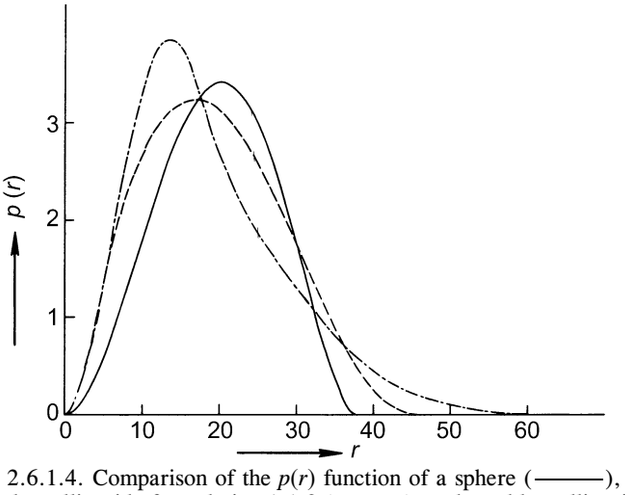

Fig. 2.6.1.4. Comparison of the $p(r)$ function of a sphere (———), a prolate ellipsoid of revolution 1:1:3 (—·—·—), and an oblate ellipsoid of revolution 1:1:0.2 (- - - -) with the same radius of gyration.

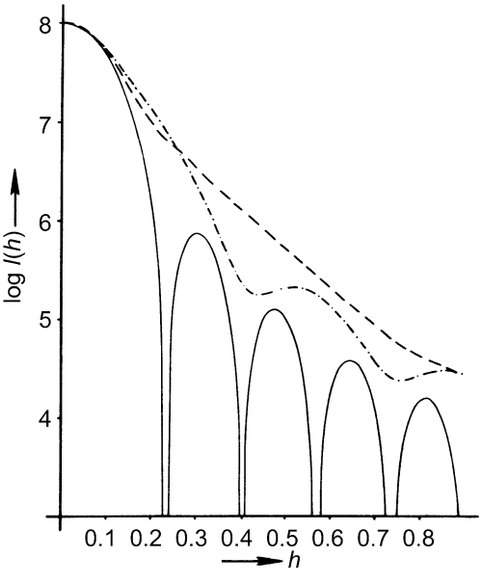

Fig. 2.6.1.5. Comparison of the $I(h)$ functions of a sphere, a prolate, and an oblate ellipsoid (see legend to Fig. 2.6.1.4).

direction with a constant cross section of arbitrary shape (long cylinders, parallelepipeds, *etc.*) The cross section A (with maximum dimension d) should be small in comparison to the length of the whole particle L:

$$d \ll L \quad L = (D^2 - d^2)^{1/2} \simeq D. \tag{2.6.1.40}$$

The scattering curve of such a particle can be written as

$$I(h) = L(\pi/h)I_c(h), \tag{2.6.1.41}$$

where the function $I_c(h)$ is related only to the cross section and the factor $1/h$ is characteristic for rod-like particles (Kratky & Porod, 1948; Porod, 1982). The cross-section function $I_c(h)$ is

$$I_c(h) = (L\pi)^{-1}I(h)h = \text{constant} \times I(h)h. \tag{2.6.1.42}$$

This function was used in the previous subsection for the determination of the cross-section parameters R_c, A, and M_c. In addition, we have

$$I_c(h) = 2\pi \int_0^\infty p_c(r)J_0(hr)\,\mathrm{d}r, \tag{2.6.1.43}$$

where $J_0(hr)$ is the zero-order Bessel function and

$$p_c(r) = \frac{1}{2\pi}\int_0^\infty I_c(h)(hr)J_0(hr)\,\mathrm{d}h \tag{2.6.1.44}$$

(Glatter, 1982*a*). The function $p_c(r)$ is the PDDF of the cross section with

$$p_c(r) = r\gamma_c(r) = \langle \Delta\rho(\mathbf{r}_c) * \Delta\rho(-\mathbf{r}_c)\rangle. \tag{2.6.1.45}$$

The symbol * stands for the mathematical operation called convolution and the symbol $\langle\ \rangle$ means averaging over all directions in the plane of the cross section. Rod-like particles with a constant cross section show a linear descent of $p(r)$ for $r \gg d$ if $D > 2.5d$. The slope of this linear part is proportional to the square of the area of the cross section,

$$\frac{\mathrm{d}p}{\mathrm{d}r} = -\frac{A^2\Delta\rho^2}{2}. \tag{2.6.1.46}$$

The PDDF's of parallelepipeds with the same cross section but different length L are shown in Fig. 2.6.1.6. The maximum corresponds to the cross section and the point of inflection r_i gives a rough indication for the size of the cross section. This is shown more clearly in Fig. 2.6.1.7, where three parallelepipeds with equal cross section area A but different cross-section dimensions are shown. If we find from the overall PDDF that the particle under investigation is a rod-like particle, we can use the PDDF of the cross section $p_c(r)$ to obtain more information on the cross section (Glatter, 1980*a*).

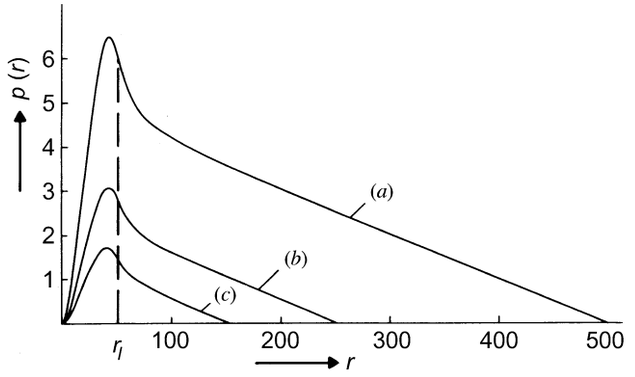

Fig. 2.6.1.6. Distance distributions from homogeneous parallelepipeds with edge lengths of: (*a*) 50 × 50 × 500 Å; (*b*) 50 × 50 × 250 Å; (*c*) 50 × 50 × 150 Å.

Flat particles. Flat particles, *i.e.* particles elongated in two dimensions (discs, flat parallelepipeds), with a constant thickness T much smaller than the overall dimensions D, can be treated in a similar way. The scattering function can be written as

$$I(h) = A\frac{2\pi}{h^2}I_t(h), \tag{2.6.1.47}$$

where $I_t(h)$ is the so-called thickness factor (Kratky & Porod, 1948) or

$$I_t(h) = (A2\pi)^{-1}I(h)h = \text{constant} \times I(h)h^2, \tag{2.6.1.48}$$

which can be used for the determination of R_t, T, and M_t. In addition, we have again:

$$I_t(h) = 2\int_0^\infty p_t(r)\cos(hr)\,\mathrm{d}r \tag{2.6.1.49}$$

and

$$p_t(r) = \gamma_t(r) - \frac{1}{\pi}\int_0^\infty I_t(h)\cos(hr)\,\mathrm{d}h$$
$$= \Delta\rho_t(r) * \Delta\rho_t(-r). \tag{2.6.1.50}$$

PDDF's from flat particles do not show clear features and therefore it is better to study $f(r) = p(r)/r$ (Glatter, 1979). The corresponding functions for lamellar particles with the same basal plane but different thickness are shown in Fig. 2.6.1.7(*b*). The marked transition points in Fig. 2.6.1.7(*b*) can be used to determine the thickness. The PDDF of the thickness $p_t(r)$ can give more information in such cases, especially for inhomogeneous particles (see below).

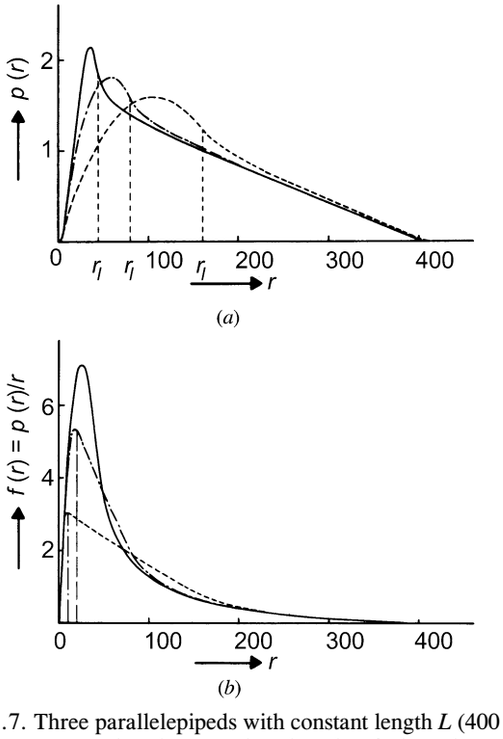

Fig. 2.6.1.7. Three parallelepipeds with constant length L (400 Å) and a constant cross section but varying length of the edges: ——— 40 × 40 Å; —·—·— 80 × 20 Å; - - - - 160 × 10 Å. (*a*) $p(r)$ function. (*b*) $f(r) = p(r)/r$.

Composite structures – aggregates, subunits. The formation of dimers can be analysed qualitatively with the $p(r)$ function (Glatter, 1979). For an approximate analysis, it is only necessary to know the PDDF of the monomer. Different types of aggregates will have distinct differences in their PDDF. Higher aggregates generally cannot be classified unambiguously. Additional information from other sources, such as the occurrence of symmetry, can simplify the problem.

Particles that consist of aggregates of a relatively large number of identical subunits show, at low resolution, the overall structure of the whole particle. At larger angles (higher resolution), the influence of the individual subunits can be seen. In the special case of globular subunits, it is possible to determine the size of the subunits from the position of the minima of the corresponding shape factors using equation (2.6.1.39) (Glatter, 1972; Pilz, Glatter, Kratky & Moring-Claesson, 1972).

2.6.1.3.2.2. *Hollow and inhomogeneous particles*

We have learned to classify homogeneous particles in the previous part of this section. It is possible to see from scattering data [$I(h)$ or $p(r)$] whether a particle is globular or elongated, flat or rod-like, *etc*., but it is impossible to determine uniquely a complicated shape with many parameters. If we allow internal inhomogeneities, we make things more complicated and it is clear that it is impossible to obtain a unique reconstruction of an inhomogeneous three-dimensional structure from its scattering function without additional *a priori* information. We restrict our considerations to special cases that are important in practical applications and that allow at least a solution in terms of a first-order approximation. In addition, we have to remember that the $p(r)$ function is weighted by the number of excess electrons that can be negative. Therefore, a minimum in the PDDF can be caused by a small number of distances, or by the addition of positive and negative contributions.

Spherically symmetric particles. In this case, it is possible to describe the particle by a one-dimensional radial excess density function $\Delta\rho(r)$. For convenience, we omit the Δ sign for excess in the following. As we do not have any angle-dependent terms, we have no loss of information from the averaging over angle. The scattering amplitude is simply the Fourier transform of the radial distribution:

$$A(h) = 4\pi \int_0^\infty r\rho(r)\frac{\sin(hr)}{h}\,\mathrm{d}r \qquad (2.6.1.51)$$

$[I(h) - A(h)^2]$ and

$$\rho(r) = \frac{1}{2\pi^2}\int_0^\infty hA(h)\frac{\sin(hr)}{r}\,\mathrm{d}h \qquad (2.6.1.52)$$

(Glatter, 1977*a*). These equations would allow direct analysis if $A(h)$ could be measured, but we can measure only $I(h)$. $\rho(r)$ can be calculated from $I(h)$ using equation (2.6.1.10) remembering that this function is the convolution square of $\rho(r)$ [equations (2.6.1.5) and (2.6.1.8)]. Using a *convolution square-root* technique, we can calculate $\rho(r)$ from $I(h)$ *via* the PDDF without having a 'phase problem' like that in crystallography; *i.e*. it is not necessary to calculate scattering amplitudes and phases (Glatter, 1981; Glatter & Hainisch, 1984; Glatter, 1988). This can be done because $p(r)$ differs from zero only in the limited range $0 < r < D$ (Hosemann & Bagchi, 1952, 1962). In mathematical terms, it is again the difference between a Fourier series and a Fourier integral.

Details of the technique cannot be discussed here, but it is a fact that we can calculate the radial distribution $\rho(r)$ from the scattering data assuming that the spherical scatterer is only of finite size. The hollow sphere can be treated either as a homogeneous particle with a special shape or as an inhomogeneous particle with spherical symmetry with a step function as radial distribution. The scattering function and the PDDF of a hollow sphere can be calculated analytically. The $p(r)$ of a hollow sphere has a triangular shape and the function $f(r) = p(r)/r$ shows a horizontal plateau (Glatter, 1982*b*).

Rod-like particles. Radial inhomogeneity. If we assume radial inhomogeneity of a circular cylinder, *i.e*. ρ is a function of the radius r but not of the angle φ or of the value of z in cylindrical coordinates, we can determine some structural details. We define $\bar{\rho}_c$ as the average excess electron density in the cross section. Then we obtain a PDDF with a linear part for $r > d$ and we have to replace $\Delta\rho$ in equation (2.6.1.46) by $\bar{\rho}_c$ with the maximum dimension of the cross section d. The $p(r)$ function differs from that of a homogeneous cylinder with the same $\bar{\rho}_c$ only in the range $0 < r \leq d$. A typical example is shown in Fig. 2.6.1.8. The functions for a homogeneous, a hollow, and an inhomogeneous cylinder with varying density $\rho_c(r)$ are shown.

Rod-like particles. Axial inhomogeneity. This is another special case for rod-like particles, *i.e*. the density is a function of the z coordinate. In Fig. 2.6.1.9, we compare two cylinders with the same size and diameter. One is a homogeneous cylinder with density $\bar{\rho}$, diameter $d = 48$ and length $L = 480$, and the other is an inhomogeneous cylinder of the same size and mean density $\bar{\rho}$, but this cylinder is made from slices with a thickness of 20 and alternating densities of $1.5\bar{\rho}$ and $0.5\bar{\rho}$, respectively. The PDDF of the inhomogeneous cylinder has ripples with the periodicity of 40 in the whole linear range. This periodicity leads to reflections in reciprocal space (first and third order in the h range of the figure).

Flat particles. Cross-sectional inhomogeneity. Lamellar particles with varying electron density perpendicular to the basal plane, where ρ is a function of the distance x from the central plane, show differences from a homogeneous lamella of the same size in the PDDF in the range $0 < r < T$, where T is the

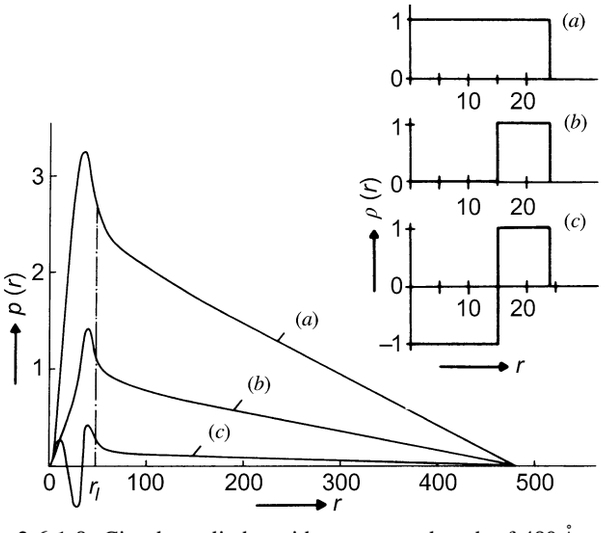

Fig. 2.6.1.8. Circular cylinder with a constant length of 480 Å and an outer diameter of 48 Å. (*a*) Homogeneous cylinder, (*b*) hollow cylinder, (*c*) inhomogeneous cylinder. The $p(r)$ functions are shown on the left, the corresponding electron-density distributions $\rho(r)$ on the right.

thickness of the lamella. An example is given in Fig. 2.6.1.10 where we compare a homogeneous lamellar particle (with $\rho = +\frac{1}{3}$) with an inhomogeneous one, $\rho_t(x)$ being a three-step function alternating between the values $+1$, -1, $+1$.

Flat particles. In-plane inhomogeneity. Lamellae with a homogeneous cross section but inhomogeneities along the basal plane have a PDDF that deviates from that of a homogeneous lamella in the whole range $0 < r < D$. These deviations are a measure of the in-plane inhomogeneites; a general evaluation method does not exist. Even more complicated is the situation that occurs in membranes: these have a pronounced cross-sectional structure with additional in-plane inhomogeneities caused by the membrane proteins (Laggner, 1982; Sadler & Worcester, 1982).

Contrast variation and labelling. An important method for studying inhomogeneous particles is the method of contrast variation (Stuhrmann, 1982). By changing the contrast of the solvent, we can obtain additional information about the inhomogeneities in the particles. This variation of the contrast is much easier for neutron scattering than for X-ray scattering because hydrogen and deuterium have significantly different scattering cross sections. This technique will therefore be discussed in the section on neutron small-angle scattering.

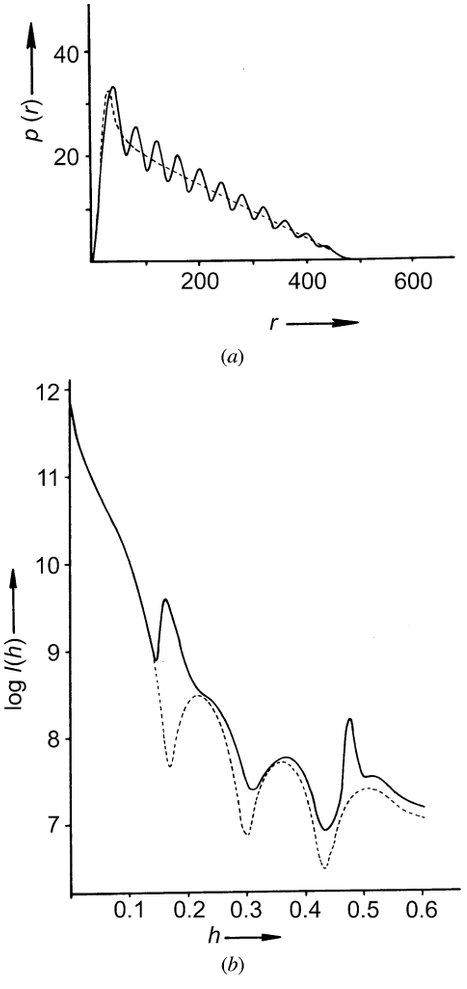

Fig. 2.6.1.9. Inhomogeneous circular cylinder with periodical changes of the electron density along the cylinder axis compared with a homogeneous cylinder with the same mean electron density. (*a*) $p(r)$ function; (*b*) scattering intensity; ——— inhomogeneous cylinder; - - - - homogeneous cylinder.

A method for distance determination with X-rays by heavy-atom labelling was developed by Kratky & Worthman (1947). These ideas are now used for the determination of distances between deuterated subunits of complex macromolecular structures with neutron scattering.

High-resolution experiments. A special type of study is the comparison of the structures of the same molecule in the crystal and in solution. This is done to investigate the influence of the crystal field on the polymer structure (Krigbaum & Kügler, 1970; Damaschun, Damaschun, Müller, Ruckpaul & Zinke, 1974; Heidorn & Trewhella, 1988) or to investigate structural changes (Ruckpaul, Damaschun, Damaschun, Dimitrov, Jänig, Müller, Pürschel & Behlke, 1973; Hubbard, Hodgson & Doniach, 1988). Sometimes such investigations are used to verify biopolymer structures predicted by methods of theoretical physics (Müller, Damaschun, Damaschun, Misselwitz, Zirwer & Nothnagel, 1984). In all cases, it is necessary to measure the small-angle scattering curves up to relatively high scattering angles ($h \simeq 30\,\mathrm{nm}^{-1}$, and more). Techniques for such experiments have been developed during recent years (Damaschun, Gernat, Damaschun, Bychkova & Ptitsyn, 1986; Gernat, Damaschun, Kröber, Bychkova & Ptitsyn, 1986; I'anson, Bacon, Lambert, Miles, Morris, Wright & Nave, 1987) and need special evaluation methods (Müller, Damaschun & Schrauber, 1990).

2.6.1.3.3. *Interparticle interference, concentration effects*

So far, only the scattering of single particles has been treated, though, of course, a great number of these are always present. It has been assumed that the intensities simply add to give the total diffraction pattern. This is true for a very dilute solution, but with increasing concentration interference effects will contribute. Biological samples often require higher concentrations for a sufficient signal strength. We can treat this problem in two different ways:

–We accept the interference terms as additional information about our system under investigation, thus observing the spatial arrangement of the particles.

–We treat the interference effect as a perturbation of our single-particle concept and discuss how to remove it.

The first point of view is the more general, but there are many open questions left. For many practical applications, the second point of view is important.

The radial distribution function. In order to find a general description, we have to restrict ourselves to an isotropic assembly of monodisperse spheres. This makes it possible to

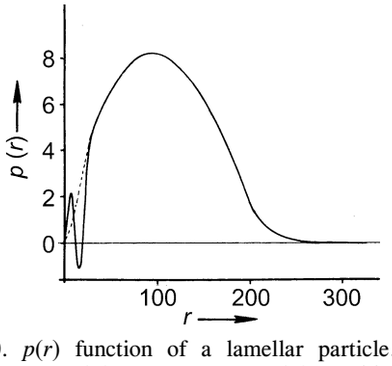

Fig. 2.6.1.10. $p(r)$ function of a lamellar particle. The full line corresponds to an inhomogeneous particle, $\rho_t(x)$ is a three-step function with the values $+1$, -1, $+1$. The broken line represents the homogeneous lamella with $\rho = +\frac{1}{3}$.

describe the situation by introducing a radial interparticle distribution function $P(r)$ (Zernicke & Prins, 1927; Debye & Menke, 1930). Each particle has the same surroundings. We consider one central particle and ask for the probability that another particle will be found in the volume element $\mathrm{d}V$ at a distance r apart. The mean value is $(N/v)\,\mathrm{d}V$; any deviation from this may be accounted for by a factor $P(r)$. In the range of impenetrability ($r < D$), we have $P(r) = 0$ and in the long range ($r \gg D$) $P(r) = 1$. So the corresponding equation takes the form

$$I(h) = NI_1(h)\left[1 + \frac{N}{V}\int_0^\infty 4\pi r^2[P(r) - 1]\frac{\sin(hr)}{hr}\,\mathrm{d}r\right]. \quad (2.6.1.53)$$

The second term contains all interparticle interferences. Its predominant part is the 'hole' of radius D, where $[P(r) - 1] = -1$. This leads to a decrease of the scattering intensity mainly in the central part, which results in a liquid-type pattern (Fig. 2.6.1.11). This can be explained by the reduction of the contrast caused by the high number of surrounding particles. Even if a size distribution for the spheres is assumed, the effect remains essentially the same (Porod, 1952). Up to now, no exact analytical expressions for $P(r)$ exist. The situation is even more complicated if one takes into account attractive or repulsive interactions or non-spherical particle shapes (orientation).

If we have a system of spheres with known size D, we can use equation (2.6.1.37) for $I_1(h)$ in equation (2.6.1.53), divide by this function, and calculate $P(r)$ from experimental data by Fourier inversion. The interference term can be used to study particle correlations of charged macromolecular solutions (Chen, Sheu, Kalus & Hoffmann, 1988).

If there are attractive forces, there will be a tendency for aggregation. This tendency may, for instance, be introduced by some steps in the procedure of preparation of biological samples. Such aggregation leads to an increase of the intensity in the central part (gas type). In this case, we will finally have a polydisperse system of monomers and oligomers. Again, there exist no methods to analyse such a system uniquely.

Elimination of concentration effects – liquid type. In most cases, the interference effect is a perturbation of our experiment where we are only interested in the particle scattering function. Any remaining concentration effect would lead to errors in the resulting parameters. As we have seen above, the effect is essential at low h values, thus influencing $I(0)$, R_g, and the PDDF at large r values.

The problem can be handled for the liquid-like type in the following way. We measure the scattering function $I(h)$ at different concentrations (typically from a few $\mathrm{mg\,ml^{-1}}$ up to about $50\,\mathrm{mg\,ml^{-1}}$). The influence of the concentration can be seen in a common plot of these scattering curves, divided by their concentrations. For large h values, these curves are identical. In the low-h range, the curves must be extrapolated to zero concentration. It depends on the problem as to whether a linear fit is sufficient or whether a second-degree polynomial has to be used. The extrapolation can be performed in a standard $I(h)/c$ *versus* h plot or in a Zimm plot $[I(h)/c]^{-1}$ *versus* h (Cleemann & Kratky, 1960; Kirste & Oberthür, 1982). The Zimm plot should be preferred when working with highly concentrated solutions (Pilz, 1982).

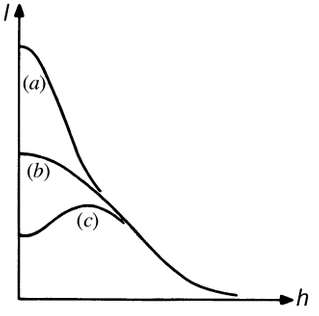

Fig. 2.6.1.11. Characteristic types of scattering functions: (*a*) gas type; (*b*) particle scattering; (*c*) liquid type.

As mentioned above, the innermost part of the scattering function is lowered and the apparent radius of gyration decreases with increasing concentration. The length of the linear range of the Guinier plot can be extended by the interference effect for non-spherical particles. Thus, an elongated linear Guinier plot is no guarantee of the completeness of the elimination of the concentration effect. Remaining interparticle interferences cannot be recognized in reciprocal space.

The PDDF is affected considerably by interparticle interference (Glatter, 1979). It is lowered with increasing distance r, goes through a negative minimum in the region of the maximum dimension D of the particle, and the oscillations vanish at larger r values. This is shown for the hard-sphere model in Fig. 2.6.1.12. The oscillations disappear when the concentration goes to zero.

The same behaviour can be found from experimental data even in the case of non-spherical data (Pilz, Goral, Hoylaerts, Witters & Lontie, 1980; Pilz, 1982).

In some cases, it may be impossible to carry out experiments with varying concentrations. This will be the case if the structure of the particles depends on concentration. Under certain circumstances, it is possible to find the particle parameters by neglecting the innermost part of the scattering function influenced by the concentration effect (Müller & Glatter, 1982).

Aggregates – gas type. When the particles show a tendency to aggregation with increasing concentration, we can follow the same procedures as discussed for the liquid type, *i.e.* perform a concentration series and extrapolate the $I(h)/c$ curves to zero concentration.

However, in most cases, the tendency to aggregation exists at any concentration, *i.e.* even at very high dilution we have a certain number of oligomers coexisting with monomers. There is no unique way to find the real particle parameters in these cases. It is not sufficient just to neglect the innermost part of the

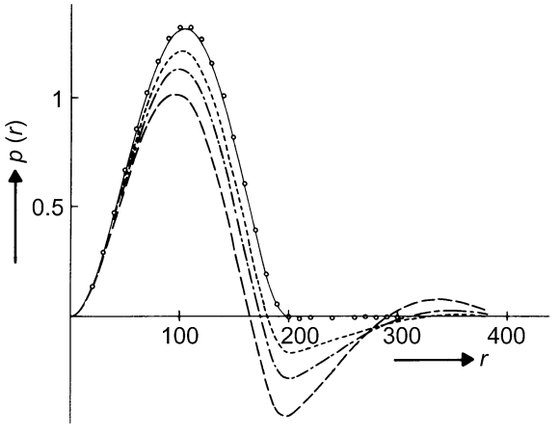

Fig. 2.6.1.12. Distance distribution – hard-sphere interference model. Theoretical $p(r)$ functions: ——— $\theta = 0$; - - - $\theta = 0.25$; —·—·— $\theta = 0.5$; — — — $\theta = 1.0$. Circles: results from indirect transformation: $\theta = 0.5$, $h_1R = 2.0$. 2% statistical noise, $D_{\max} = 300\,\text{Å}$, $\Delta R_g = 0.5\%$, $\Delta I_0 = 1.2\%$.

scattering function because that leads to an increasing loss of essential information about the particle (monomer) itself.

2.6.1.4. *Polydisperse systems*

In this subsection, we give a short survey of the problem of polydispersity. It is most important that there is no way to decide from small-angle scattering data whether the sample is mono- or polydisperse. Every data set can be evaluated in terms of monodisperse or polydisperse structures. Independent *a priori* information is necessary to make this decision. It has been shown analytically that a certain size distribution of spheres gives the same scattering function as a monodisperse ellipsoid with axes a, b and c (Mittelbach & Porod, 1962).

The scattering function of a polydisperse system is determined by the shape of the particles and by the size distribution. As mentioned above, we can assume a certain size distribution and can determine the shape, or, more frequently, we assume the shape and determine the size distribution. In order to do this we have to assume that the scattered intensity results from an ensemble of particles of the same shape whose size distribution can be described by $D_n(R)$, where R is a size parameter and $D_n(R)$ denotes the number of particles of size R. Let us further assume that there are no interparticle interferences or multiple scattering effects. Then the scattering function $I(h)$ is given by

$$I(h) = c_n \int_0^\infty D_n(R) R^6 i_0(hR)\, \mathrm{d}R, \qquad (2.6.1.54)$$

where c_n is a constant, the factor R^6 takes into account the fact that the particle volume is proportional to R^3, and $i_0(hR)$ is the normalized form factor of a particle size R. In many cases, one is interested in the mass distribution $D_m(R)$ [sometimes called volume distribution $D_c(R)$]. In this case, we have

$$I(h) = c_m \int_0^\infty D_m(R) R^3 i_0(hR)\, \mathrm{d}R. \qquad (2.6.1.55)$$

The solution of these integral equations, *i.e.* the computation of $D_n(R)$ or $D_m(R)$ from $I(h)$, needs rather sophisticated numerical or analytical methods and will be discussed later.

The problems of interparticle interference and multiple scattering in the case of polydisperse systems cannot be described analytically and have not been investigated in detail up to now. In general, interference effects start to influence data from small-angle scattering experiments much earlier, *i.e.* at lower concentration, than multiple scattering. Multiple scattering becomes more important with increasing size and contrast and is therefore dominant in light-scattering experiments in higher concentrations.

A concentration series and extrapolation to zero concentration as in monodisperse systems should be performed to eliminate these effects.

2.6.1.5. *Instrumentation*

X-ray sources are the same for small-angle scattering as for crystallographic experiments. One can use conventional generators with sealed tubes or rotating anodes for higher power. For the vast majority of applications, an X-ray tube with copper anode is used; the wavelength of its characteristic radiation (Cu $K\alpha$ line) is 0.154 nm. Different anode materials emit X-rays of different characteristic wavelengths.

X-rays from synchrotrons or storage rings have a continuous wavelength distribution and the actual wavelength for the experiment is selected by a monochromator. The intensity is much higher than for any type of conventional source but synchrotron radiation is available only at a few places in the world. Reviews on synchrotron radiation and its application have been published during recent years (Stuhrmann, 1978; Holmes, 1982; Koch, 1988). In these reviews, one can also find some remarks on the general principles of the systems including cameras and special detectors.

2.6.1.5.1. *Small-angle cameras*

General. In any small-angle scattering experiment, it is necessary to illuminate the sample with a well defined flux of X-rays. The ideal condition would be a parallel monochromatic beam of negligible dimension and very high intensity. These theoretical conditions can never be reached in practice (Pessen, Kumosinski & Timasheff, 1973). One of the main reasons is the fact that there are no lenses as in the visible range of electromagnetic radiation. The refractive index of all materials is equal to or very close to unity for X-rays. On the other hand, this fact has some important advantages. It is, for example, possible to use circular capillaries as sample holders without deflecting the beam. There are different ways of constructing a small-angle scattering system. Slit, pinhole, and block systems define a certain area where the X-rays can pass. Any slit or edge will give rise to secondary scattering (parasitic scattering). The special construction of the instrument has to provide at least a subspace in the detector plane (plane of registration) that is free from this parasitic scattering. The crucial point is of course to provide the conditions to measure at very small scattering angles.

The other possibility of building a small-angle scattering system is to use monochromator crystals and/or bent mirrors to select a narrow wavelength band from the radiation (important for synchrotron radiation) and to focus the X-ray beam to a narrow spot. These systems require slits in addition to eliminate stray radiation.

Block collimation – Kratky camera. The Kratky (1982*a*) collimation system consists of an entrance slit (edge) and two blocks – the *U*-shaped centre piece and a block called *bridge*. With this system, the problem of parasitic scattering can be largely removed for the upper half of the plane of registration and the smallest accessible scattering angle is defined by the size of the entrance slit (see Fig. 2.6.1.13). This system can be integrated in an evacuated housing (Kratky compact camera) and fixed on the top of the X-ray tube. It is widely used in many laboratories for different applications. In the Kratky system, the X-ray beam has a rectangular shape, the length being much larger than the width. Instrumental broadening can be corrected by special numerical routines. The advantage is a relatively high primary-beam intensity. The main disadvantage is that it cannot be used in special applications such as oriented systems where

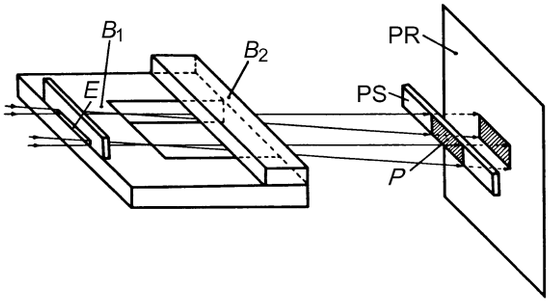

Fig. 2.6.1.13. Schematic drawing of the block collimation (Kratky camera): E edge; B_1 centre piece; B_2 bridge; P primary-beam profile; PS primary-beam stop; PR plane of registration.

references